INTERNATIONAL JOURNAL OF HYDROGEN ENERGY 40 (2015) 13506–13517

Available online at www.sciencedirect.com

ScienceDirect

journal homepage: www.elsevier.com/locate/he

Role of aluminum chloride on the reversible hydrogen storage properties of the Li–N–H system

Luisa Fernández Albanesi [a], *Sebastiano Garroni* [b], *Pierre Arneodo Larochette* [a], *Pau Nolis* [c], *Gabriele Mulas* [b], *Stefano Enzo* [b], *María Dolors Baró* [d], *Fabiana C. Gennari* [a,*]

[a] *Centro Atómico Bariloche (CNEA) e Instituto Balseiro (UNCuyo), R8402AGP Bariloche, Río Negro, Argentina*
[b] *Department of Chemistry and Pharmacy, University of Sassari and INSTM, Via Vienna 2, I-07100, Sassari, Italy*
[c] *Servei de Ressonància Magnètica Nuclear (SeRMN), Universitat Autònoma de Barcelona, E-08193, Bellaterra, Spain*
[d] *Departament de Física, Universitat Autònoma de Barcelona, E-08193, Bellaterra, Spain*

ARTICLE INFO

Article history:
Received 31 May 2015
Received in revised form
30 July 2015
Accepted 7 August 2015
Available online 1 September 2015

Keywords:
Hydrogen storage material
Lithium amide/Lithium hydride system
Aluminum chloride
Kinetics and thermodynamics properties
XRPD
ss-MAS-NMR

ABSTRACT

In order to understand the role of $AlCl_3$ addition on the Li–N–H system, we have systematically investigated the hydrogen sorption kinetics and the reactions between $LiNH_2$–LiH and $AlCl_3$ additive with a multitechnique approach involving differential scanning calorimetry (DSC), hydrogen volumetric measurements, X-ray powder diffraction (XRPD), Fourier transform infrared analysis (FTIR) and solid-state nuclear magnetic resonance (NMR). Different interactions were identified as a function of the amount of added $AlCl_3$. For low $AlCl_3$ addition (0.03 mol), the Al^{3+} is incorporated into the interstitial sites by the $LiNH_2$ structure. When $AlCl_3$ amount increased (0.08 and 0.13 mol), the formation of new amide-chloride phases were detected by XRPD and indexed with cubic and hexagonal Li–Al–N–H–Cl geometries. Occurrence of such new phases was also confirmed by FTIR and NMR. The formation of these new Li–Al–N–H–Cl phases modifies the kinetics as well as the thermodynamic behavior of the original Li–N–H system. Interesting, in all $AlCl_3$-doped composites, hydrogen was stored reversibly with faster sorption kinetics than un-doped Li–N–H system and with a significant reduction of NH_3 emission. This improvement can be associated with the Al^{3+} incorporation into $LiNH_2$ that promotes the migration of Li^+, while for high $AlCl_3$ doping, the formation of new phases Li–Al–N–H–Cl also weakens the N–H bond.

Copyright © 2015, Hydrogen Energy Publications, LLC. Published by Elsevier Ltd. All rights reserved.

Introduction

One of the major technological challenges associated with the use of hydrogen as energy carrier is the development of an efficient and safe manner to store hydrogen. The ability of different metals and alloys to absorb and store hydrogen reversibly in the solid-state is known and has been studied since several decades. However, the searching for higher gravimetric efficiency in the storage materials raised the

* *Corresponding author*. Instituto Balseiro (UNCuyo), Centro Atómico Bariloche (CNEA) and Consejo Nacional de Investigaciones Científicas y Técnicas (CONICET), Av. Bustillo 9500, R8402AGP-S. C. de Bariloche, Argentina. Tel.: +54 2944 445118; fax: +54 2944 445190.
E-mail address: gennari@cab.cnea.gov.ar (F.C. Gennari).
http://dx.doi.org/10.1016/j.ijhydene.2015.08.030
0360-3199/Copyright © 2015, Hydrogen Energy Publications, LLC. Published by Elsevier Ltd. All rights reserved.

interest to study complex hydrides of light elements, such as alanates $[AlH_4]^-$, borohydrides $[BH_4]^-$ and amides $[NH_2]^-$ [1–11]. In fact, since the pioneering work of Chen et al. [8] metal-N-H systems are known to be one of the most promising materials for hydrogen storage. These authors reported that the reaction between lithium amide ($LiNH_2$) and LiH releases 6.5 wt.% of hydrogen upon production of lithium imide (Li_2NH) according to the following reaction

$$LiNH_2(s) + LiH(s) \leftrightarrow Li_2NH(s) + H_2(g) \quad (1)$$

The reaction is reversible under moderate pressures (lower than 5.0 MPa of hydrogen) and temperatures (~300 °C). However, the slow sorption kinetics under these experimental conditions remains a serious limitation to be overcome. Different strategies such as size reduction by ball milling or nanoconfinement [12,13], addition of metal catalysts and complex borohydrides [11,14–17] and/or partial substitution of lithium by other metal [10,18,19], have been inspected to improve the hydrogen sorption performance of the $LiNH_2$–LiH system. However, kinetic constraints have been partially alleviated but not totally eliminated.

In particular, recent works have been devoted to enhance the hydrogen sorption behavior by doping the Li–N–H with different metal halides [20–23]. Zhang et al. [20] investigated the addition of chloride ion into $LiNH_2$ via mixing LiCl and $LiNH_2$. The introduction of chloride ion resulted in a reduction in the decomposition temperature of $LiNH_2$. These authors explained that the interaction between chloride ion and $LiNH_2$, which is dependent on the contact between the surfaces of LiCl and $LiNH_2$ particles, weakens the bond between Li^+ and $[NH_2]^-$. Leng et al. [21] showed significant improvement in the desorption properties of the Li–N–H system by the $MgCl_2$ addition. Three different mechanisms were proposed on the basis of the amount of $MgCl_2$ added: i) when $MgCl_2 < 4$ mol%, it acts as NH_3 sorbent; ii) when $MgCl_2 > 4$ mol%, formation of Mg^{2+} solid solution is evidenced; iii) for $MgCl_2 > 25$ mol%, the system undergoes a reaction with $LiNH_2$ by changing the composite from $LiNH_2$–LiH into LiH-0.5$Mg(NH_2)_2$ system. Furthermore, Anderson et al. [22] reported the combination of LiX (X = Cl, Br, I) with $LiNH_2$ to form amide-halide phases. These new systems were able to release hydrogen more rapidly than $LiNH_2$ itself, with practically undetectable NH_3 emission. Preliminary conductivity measurements indicated that the most conducting amide-halide phases were the quickest to release hydrogen on heating. Therefore, those additives able to improve Li^+ mobility (creation of bulk defects) [23] and/or to modify the interaction between Li^+ and $[NH_2]^-$ by cation or anion substitution, could induce improved hydrogen storage properties in the Li–N–H system.

Our recent studies have also pointed out that the $AlCl_3$ addition (0.03 mol) improve the absorption/desorption rates, hydrogen storage capacity and stability under hydrogen cycling of the $LiNH_2$-1.6LiH composite [24]. Moreover, a suppression of ammonia release was observed for the $AlCl_3$ doped $LiNH_2$-1.6LiH composite. These results were associated with the formation of a Li–Al–N–H amide after milling, which is reversible during hydrogen cycling. It was demonstrated that the inclusion of Al^{3+} in the $LiNH_2$ structure modifies the thermodynamic properties of the $LiNH_2$–LiH system, which could be the main reason for the improvement of hydrogen sorption behavior. No catalytic role of Al-containing additive was revealed [24].

In the present work we continue the study and investigate different $LiNH_2$-1.6LiH-x$AlCl_3$ composites (where $x = 0.03$, 0.08 and 0.13 mol, respectively) with the goal of understanding the role of $AlCl_3$ in the improvement of hydrogen storage properties of the $LiNH_2$-1.6LiH mixture. The reaction pathways and the possible intermediates formed during milling, posterior heating under hydrogen pressure and hydrogen desorption/absorption, were investigated and the results discussed.

Experimental

Samples were prepared by ball milling a mixture of $LiNH_2$ (Aldrich, 95%) and LiH (Fluka, 95%) in 1:1.6 molar ratio (denoted LN). The additive $AlCl_3$ (Merck, 98%) was incorporated by milling in the final chemical composition $LiNH_2$-1.6LiH-x$AlCl_3$ (x = 0.03, 0.08 and 0.13 mol). These samples were denoted LN1, LN2 and LN3, respectively. The amount of LiH was added in excess with respect to Reaction (1) to avoid, or minimize, the emission of NH_3 [24]. The amount of $AlCl_3$ was selected based on previous work [24] to progressively modify the ratio respect to $LiNH_2$–LiH composite. The ball milling was performed in a planetary mill (Fritsch Pulverisette 6) under 0.1 MPa of argon atmosphere during 5 h. The milling conditions were 400 rpm with a ball/sample mass ratio of 40:1. To avoid temperature ramping during milling, each 15 min running was followed by an interval of 10 min pause. Samples were prepared and manipulated inside an argon-filled glove box equipped with a circulative purification system to prevent moisture and oxygen contamination, with O_2 and H_2O concentrations kept below 1 ppm. During milling of the $LiNH_2$-1.6LiH-0.13$AlCl_3$ composite, a clear increment in the gas pressure of the milling chamber was observed due to the hydrogen production. No NH_3 emission was detected by gas-FTIR analysis of the milling atmosphere. Then, if NH_3 was formed, we surmise that it is present in a lower amount than the detection limits (~2 ppm per volume, under experimental conditions used).

Pressure composition isotherms (PCIs) and hydrogen desorption/absorption kinetics were measured using a modified Sieverts-type device, coupled with a mass flow controller. First, the sample was heated up to the selected reaction temperature under hydrogen pressure and kept at this temperature for 30 min. Then, the sample was dehydrogenated (first desorption measurement) and consecutively rehydrogenated (first absorption measurement). For PCI measurement of dehydrogenation, a programmed hydrogen amount was extracted from the system using the mass flow controller. When the system is considered under equilibrium conditions, one point of the PCI curve is saved. The hydrogen contents were reported as weight percent with respect to the mass of the $LiNH_2$–LiH mixture (1:1 mol ratio) present in the total mass of $LiNH_2$-1.6LiH-x$AlCl_3$, to compare directly with Reaction (1).

X-ray powder diffraction (XRPD) measurements were conducted with a PANaytical Empyrean instrument using Cu Kα radiation. The generator was working at 40 kV and 45 mA and the goniometer equipped with a graphite monochromator

in the diffracted beam. The samples were mounted in an especially airtight holder to avoid any oxidation process of the powders. Phase abundance and microstructural parameters were evaluated by fitting the XRPD patterns by Rietveld method using the software MAUD [25,26].

Fourier transform infrared spectroscopy (FTIR) measurements were carried out using a Perkin Elmer Spectrum 400 instrument, using MCT detector. The gases released after milling and during dehydrogenation of the samples were collected in a degassed quartz optical cell with KBr windows and optical length of 9 cm. The gas phase spectra at room temperature were taken, with a resolution of 0.5 cm^{-1}. Solid-state IR spectra were obtained in the range of 1000–4000 cm^{-1} using a specially designed cell, with a resolution of 4 cm^{-1}. Selected samples were grounded with dry KBr under purified argon atmosphere and pressed to pellets. Handling was done inside the glove box to avoid contact with air.

The thermal behavior of the samples was analyzed by DSC (TA Instruments) using a heating ramp of 5 °C/min and argon flow rate of 122 ml/min. The heat flow was calculated with respect to the total mass of the $LiNH_2$–LiH mixture (1:1 mol ratio), to compare directly with Reaction (1). About 5–7 mg of sample was loaded into aluminum capsules hermetically closed in the glove box. The Kissinger method was employed to determine the apparent activation energy of the dehydrogenation process, represented by the following equation:

$$d\left[\ln\left(\frac{\beta}{T_{p^2}}\right)\right]\Big/d\left(\frac{1}{T_p}\right)=\frac{-E_a}{R} \quad (2)$$

where T_p is the peak temperature of the endothermic effect, β is the heating rate, E_a is the activation energy and R is the gas constant. The slope of the fitted straight line corresponds to the activation energy (E_a) for the reaction. The DSC technique was employed to obtain the maximum reaction rate temperatures at various heating rates (1, 2, 5, 15 and 20 or 25 °C/min).

Magic-Angle Spinning (MAS) solid-state ^{27}Al and ^{7}Li NMR experiments were performed at room temperature on a Bruker Advance 400 MHz spectrometer with a wide-bore 9.4 T magnet and by employing a boron-free Bruker 4 mm CPMAS probe. The spectral frequencies were 104.28 MHz and 155.52 MHz for the nucleus of ^{27}Al and ^{7}Li, respectively. The NMR chemical shifts were reported in parts per million (ppm) externally referenced to $Al(NO_3)_3$ (^{27}Al) and LiCl (^{7}Li), respectively. The powder materials were packed into the 4 mm ZrO_2 rotors in an argon-filled glove box and sealed with tight-fitting Kel-F caps. Sample spinning was acted using dry nitrogen gas. MAS experiments were performed at sample rotation frequencies of 10 and 12 kHz. Spectra were acquired at 20 °C, with the temperature controlled by a Bruker BCU unit. All recorded spectra were analyzed by MestreNova software.

Results and discussions

Sorption properties of as-milled $LiNH_2$-1.6LiH- x$AlCl_3$ composite (x = 0.03, 0.08, 0.13)

To evaluate the effect of $AlCl_3$ addition on dehydrogenation of the $LiNH_2$-1.6LiH composite, samples with different $AlCl_3$ content were prepared and their hydrogen release behavior compared using non-isothermal and isothermal measurements, respectively. Fig. 1 displays the DSC curves obtained from the doped $AlCl_3$ samples (LN1, LN2 and LN3). For comparison purposes, the DSC curve of the pristine LN composite is also presented in Fig. 1(A). Only one endothermic peak, ascribable to the dehydrogenation process, is observed for all composites. The peak maximum temperature of the $AlCl_3$-doped composites is reduced by 20–30 °C with respect to the un-doped LN (260 °C) and although the hydrogen release starts approximately at the same temperature (about 180 °C) for all samples, in the $AlCl_3$-doped composites is completed in a narrow temperature range. This may indicate that $AlCl_3$ facilitates the reaction kinetics in comparison with the un-doped composite. Our previous study demonstrated that minor amounts of NH_3 were detected during LN heating from 280 °C (in the order of 500 ppm), which increases at 300 °C (1300 ppm) [24]. However, no NH_3 emission is noticed during heating of any $AlCl_3$ doped $LiNH_2$-1.6LiH composites up to 350 °C, using the same gas-FTIR technique. The reduction/elimination of ammonia emission is attributed to the presence of $AlCl_3$, which modifies the reaction kinetics of LN. Similar experimental evidence was obtained by addition of halides to Li–N–H and Li–Mg–N–H composites [21,22,27]. On the other hand, an exothermic peak at 130 °C is observed for LN3 mixture, which will be analyzed in the next section.

In the case of the isothermal measurements, the as-milled samples were first heated under 0.7 MPa of hydrogen pressure up to 300 °C and kept at this temperature for 0.5 h Fig. 2A shows dehydrogenation curves obtained for doped and un-doped composites at 300 °C and 0.02 MPa of hydrogen. Hydrogen release evidences the beneficial effect of the different amounts of $AlCl_3$ doping the $LiNH_2$-1.6LiH composite. From Fig. 2A it can be seen that the hydrogen desorption from doped LN is faster than $AlCl_3$-free sample. In addition, by analyzing the slope of the initial parts of the hydrogen desorption curves (see Fig. 2A, region between 0.01 and 0.15 wt.%), the desorption rates for LN1, LN2 and LN3 were estimated (1.4, 2.2 and 2.0 wt.%/min, respectively). These values are about three-fold and six-fold factor higher with respect to that of the un-doped LN sample (0.36 wt.%/min), evidencing that the dehydrogenation kinetics of the LN composite is effectively improved by the $AlCl_3$ addition. On the other hand, the amount of hydrogen released after 1 h decreases from 5.0 wt.% for LN1 to 4.3 and 3.9 wt.% for LN2 and LN3, respectively, in comparison with 3.5 wt.% for un-doped material. These values are in good correlation with the theoretical hydrogen storage capacities calculated with respect to the mass of the $LiNH_2$-1.6LiH doped mixtures which are corresponding to 5.1 (~98%), 4.3 (~100) and 3.8 (~100) wt.% for LN1, LN2 and LN3, respectively. Taking into account that hydrogen partial release occurred during milling of LN3, the agreement between the theoretical and experimental hydrogen storage capacity indicates that LN3 was hydrogenated during the thermal treatment under hydrogen prior to the dehydrogenation process.

After the first desorption step, samples were submitted to hydrogen uptake under 0.7 MPa of hydrogen at 300 °C to assess the reversibility of the system (Fig. 2B). Hydrogen storage capacity and hydrogen absorption/desorption rate displayed

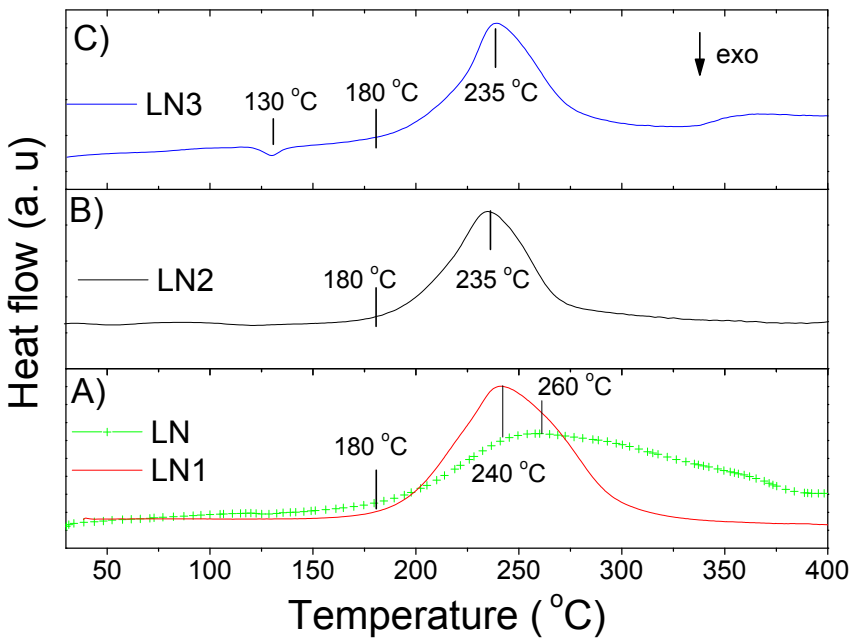

Fig. 1 – DSC curves of: A) LN and LN1, B) LN2, C) LN3.

good stability after seven cycles for LN1 (4.8 wt.%) [24]. In contrast, the hydrogen storage behavior of LN change was deteriorating during cycling due to NH_3 emission from 280 °C [24]. Furthermore, reasonable reversibility was also observed for LN2 and LN3 composites (3.9 and 3.6 wt.%, respectively), confirming, at the best of our knowledge, that $AlCl_3$ addition improves both the desorption/absorption rate and the hydrogen storage reversibility of the $LiNH_2$-1.6LiH system with respect to the un-doped material.

Taking into account that $AlCl_3$ addition improves the hydrogen storage properties of LN, the interactions between $AlCl_3$ and $LiNH_2$–LiH during milling, heating under hydrogen and vacuum should be inspected. Our attention has been then focused on the LN2 and LN3 samples.

Role of $AlCl_3$ addition in the $LiNH_2$-1.6LiH composite

To understand the role of $AlCl_3$ in the dehydrogenation step of the $LiNH_2$-1.6LiH composite, the possible interactions between the reactants during both the milling and after thermal treatment at 300 °C and 0.7 MPa of hydrogen for 0.5 h, were investigated. Fig. 3A and B exhibit the XRPD patterns of the $AlCl_3$-doped $LiNH_2$-1.6LiH systems, obtained after ball milling and thermal treatment, respectively. For the LN1 sample

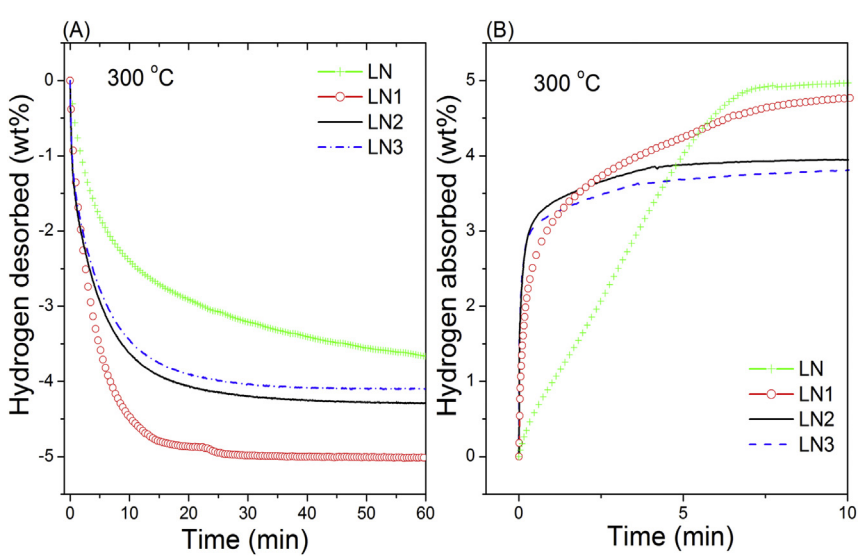

Fig. 2 – Isothermal hydrogen desorption (A) and absorption (B) of un-doped and $AlCl_3$ doped $LiNH_2$-1.6LiH composites (300 °C, P_d = 0.02 MPa and P_a = 0.7 MPa).

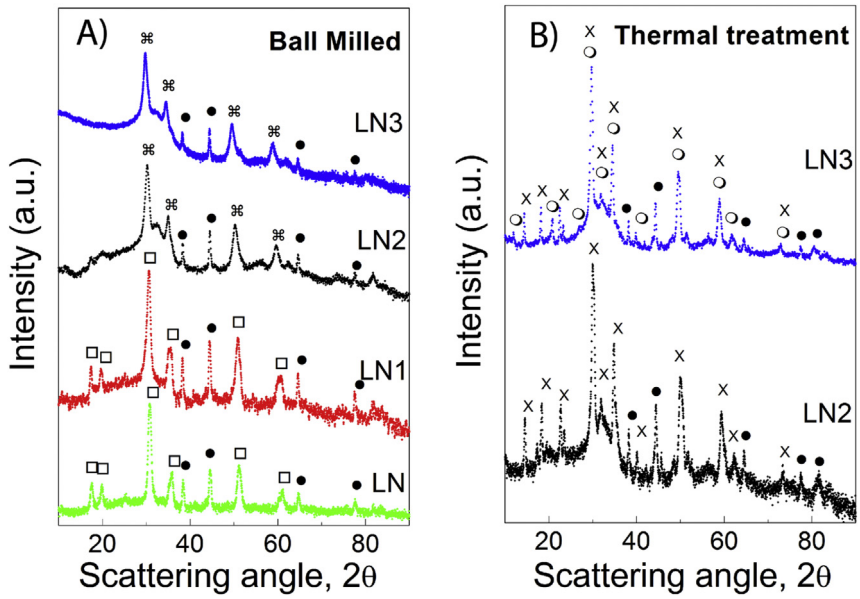

Fig. 3 – XRPD patterns of: A) LN, LN1, LN2 and LN3 after ball milling, B) LN2 and LN3 after thermal treatment at 300 °C and 0.7 MPa of hydrogen. Symbols: ❑ $LiNH_2$, ● LiH, ⌘ FCC phase, X Trigonal/hexagonal amide-halide-type phase, ○ Cubic $I2_13$ amide-halide-type phase.

(Fig. 3A), the $LiNH_2$ and LiH phases are still present in the mixture upon mechanical treatment. The Rietveld analysis (see Fig. S1 in supporting information) suggests that there is no formation of new phases due to the mechanical processing. A pronounced broadening of the $LiNH_2$ peaks was observed ascribed to crystallite size refinement (24 nm) and to the increase of microstrain. From the X-ray investigation, the evaluated amount of the $LiNH_2$ and LiH phases is around 78 and 22 wt.%, respectively, in agreement with the initially weighted composition (Table T1, supporting information). Remarkably, in correspondence to the doped samples (see Fig. S1) there is a clear shift of the most intense LiNH2 Bragg reflections towards lower angles with respect to LN, indicating that the $AlCl_3$ doping result in expansion of the lattice cell. In fact, for low $AlCl_3$ doping this phenomenon may be ascribed to the incorporation of Al^{3+} into the interstitial sites of the $LiNH_2$ lattice, promoted by the mechanical treatment (see Table 1 in supporting information), leading to the formation of a solid solution $LiNH_2$–$AlCl_3$. Considering the structural representation for $LiNH_2$ proposed by David et al. [23], lithium amide may be regarded as an ordered (a × a × 2a) form of cubic lithium imide with the Li ions in $LiNH_2$ occupying half the possible tetrahedral sites of Li_2NH. In this scheme, the Al^{3+} ions could replace sites normally reserved for Li^+ (in the cubic description, 50% are empty). To keep electro neutrality, the Cl^- ions could occupy the other empty sites. Due to the short Cl–Al distance, a lattice parameter increase of the imide-like phase is observed.

On the contrary, in the XRPD pattern of as-milled LN3, the low angle peaks corresponding to $LiNH_2$, seem to disappear completely and a series of Bragg reflections emerged, indexed with a FCC type sequence. However, for the as-milled LN1 and LN2, the peaks at low angles associated with $LiNH_2$ can not be neglected. This difference indicates that during the milling, in the case of LN3, a reaction has occurred inducing the appearance of a new arrangement and/or a new phase. Moreover, as $AlCl_3$ amount increase, the XRPD pattern background grows in the range of $2\theta = 20$–$40°$, suggesting the existence of an amorphous phase. From the analysis of Fig. 3A it is clear that the amount of amorphous component increases with the content of doping agent.

Thermal treatment under hydrogen of the as-milled LN2 and LN3 composites produces an increase of crystallinity and a reduction or elimination of the amorphous phase, which helps to clarify the interactions between reactants (Fig. 3B). A detailed inspection of the XRPD patterns of the LN2 and LN3 composites shows that some peaks at low angles are not correlated with those peaks of $LiNH_2$ structure. In fact, these XRPD patterns look completely different with respect to those of the LN and LN1 samples. For the LN2 composite, a new set of peaks can be indexed, with lattice parameters $a = 9.7020$ Å and $c = 8.9024$ Å in the hexagonal settings with *R*3 space group, similar to the phase ($Li_4(NH_2)_3Cl$) reported by Anderson et al. [22]. Apparently, this phase was not formed during milling but its formation is favored by thermal treatment at 300 °C under 0.7 MPa of hydrogen for 0.5 h. In the case of the LN3 sample after thermal treatment (Fig. 3B), in addition to the peaks associated with the trigonal/hexagonal phase, a new set of peaks can be identified. These peaks can be indexed as belonging to a cubic habit and compatible with a $I2_13$ space group, similar to that amide-halide phase reported by Anderson et al. ($Li_4(NH_2)_3Cl$) [22]. Again, the thermal treatment favors the unambiguous identification of the new type amide-chloride phase, containing aluminum. According to Anderson et al. [22,27], the $Li_4(NH_2)_3Cl$ type-phases were synthesized by heating of $3LiNH_2$–LiCl mixture up to 400 °C. They observed that after 1 h of heating, the trigonal/hexagonal phase was obtained. Longer heating times of around 12 h favored the

formation of a new phase with same composition, but with body centered cubic lattice. Then, trigonal/hexagonal and cubic $Li_4(NH_2)_3Cl$ phases are related. In order to clarify the reactivity of $AlCl_3$ with $LiNH_2$-1.6LiH composite and to obtain additional evidence of the formation of the $Li_4(NH_2)_3Cl$ phases, FTIR and NMR studies were performed on the multi-component system. Fig. 4 shows FTIR of the x$AlCl_3$-doped $LiNH_2$-1.6LiH composites after ball milling (Fig. 4A) and after thermal treatment at 300 °C under 0.7 MPa of hydrogen for 0.5 h (Fig. 4B). For comparison the spectra of un-doped sample was also included. The N–H stretches of $LiNH_2$ at 3315 and 3260 cm^{-1} are clearly identified in the LN and LN1 composites, corresponding to asymmetric and symmetric stretching of the N–H bonds, respectively. As the amount of $AlCl_3$ increases in the $LiNH_2$-1.6LiH composites (LN2 and LN3), the peak positions corresponding to N–H vibrations shift to wave numbers (3297 and 3245 cm^{-1} for LN3) lower than those of the un-doped material. In addition, for the as-milled LN3 sample a band at 3365 cm^{-1} is clearly identified in the spectrum. These IR bands cannot be clearly assigned to any known Li–Al–N–H or Li–Al–N–H–Cl compounds. Indeed, these wave numbers are still high (above 3200 cm^{-1}) to account for an imide formation. Similar bands were previously reported by Xiong et al. [28] due to the formation of an intermediate with the proposed $Li_3AlN_2H_4$ chemical composition during dehydrogenation of $2LiNH_2$–$LiAlH_4$. Additionally, analogous bands were observed after 48 h of milling of the $LiAl(NH_2)_4$:4LiH mixture [29] and after 24 h of milling of the Li_2AlH_6–$LiNH_2$ mixture [10].

FTIR spectra of the thermal treated samples help to clarify the shape and intensity of the bands at 3297 and 3245 cm^{-1} observed in the $AlCl_3$ doped material (Fig. 4B). Certainly, the NH_2^- group remains intact after milling with $AlCl_3$ and subsequent thermal treatment. However, N–H bands are shifted at lower numbers than that of the un-doped material. These FTIR bands are in the same position of those observed in the Raman spectra reported by Anderson et al. for amide-halides of chemical formula $Li_4(NH_2)_3Cl$ and $Li_3Mg_{0.5}(NH_2)_3Cl$, suggesting analogous structural characteristics with these phases [22]. In particular, the FTIR spectra for LN2 and LN3 composites after 0.5 h of thermal treatment under hydrogen, shows two incipient asymmetric and symmetric stretches that can be associated with the $Li_4(NH_2)_3Cl$ hexagonal phase, indicating different NH_2^- environments [22]. The lowering in the wave numbers of the new phase in the Li–Al–N–H–Cl system shows that the N–H bond is longer and therefore weaker in the $LiNH_2$-1.6LiH-x$AlCl_3$ composites compared to $LiNH_2$. Considering that the hydrogen release involves the N–H bond breaking, a lower temperature of hydrogen desorption is expected. These results provide evidence of the structural changes occurring in the material prior to the improved dehydrogenation process observed (Fig. 2A). It is interesting to remark that after thermal treatment, the band at 3365 cm^{-1} practically disappears. Then, the experimental evidence suggests that the temperature induces a rearrangement of the Li–Al–N–H–Cl structure with respect to the as-milled samples.

The FTIR spectra of the $AlCl_3$ doped $LiNH_2$-1.6LiH composites after dehydrogenation (Fig. 5A) and rehydrogenation (Fig. 5B) were analyzed. For comparison, the spectrum of the LN composite is also shown. In the desorbed LN sample, a peak at 3180 cm^{-1} is observed, characteristic of the Li_2NH compound, implying the conversion of $LiNH_2$ into Li_2NH. The band at 3260 cm^{-1} is associated with the uncompleted desorption of the $LiNH_2$ in the LN composite (Fig. 2A). The N–H stretch at 3180 cm^{-1} for dehydrogenated LN shifts to lower wave numbers (3160 and 3150 cm^{-1} for LN2 and LN3, respectively) with the increase of $AlCl_3$ doping (Fig. 5A). In the rehydrogenated LN sample (Fig. 5B), N–H stretching vibrations of $LiNH_2$ are again detected at 3260 and 3315 cm^{-1}, demonstrating the rehydrogenation of the un-doped composite. Similar situations occur with the $LiNH_2$-1.6LiH samples doped with x$AlCl_3$ after rehydrogenation: the bands at 3297

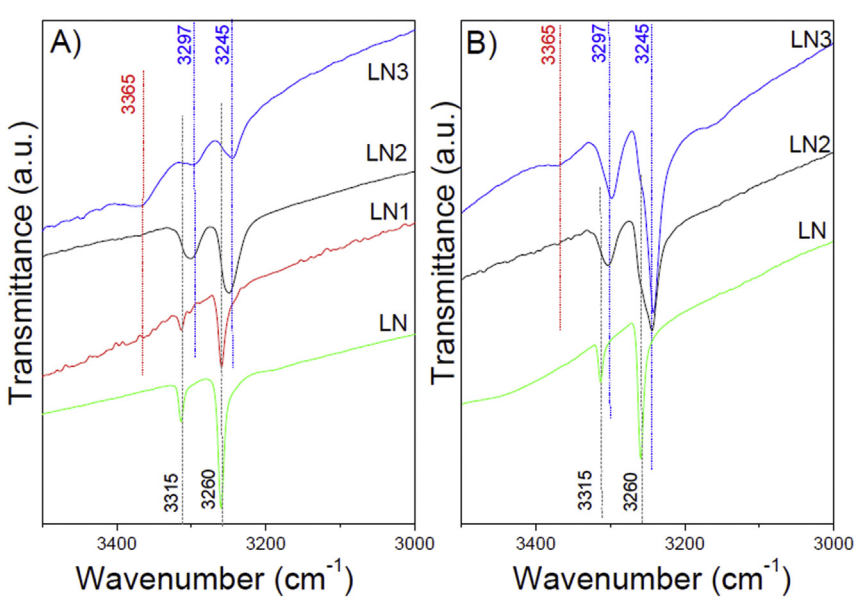

Fig. 4 – FTIR spectra of $AlCl_3$ doped $LiNH_2$-1.6LiH composite (A) after ball milling and (B) after thermal treatment at 300 °C and 0.7 MPa of hydrogen.

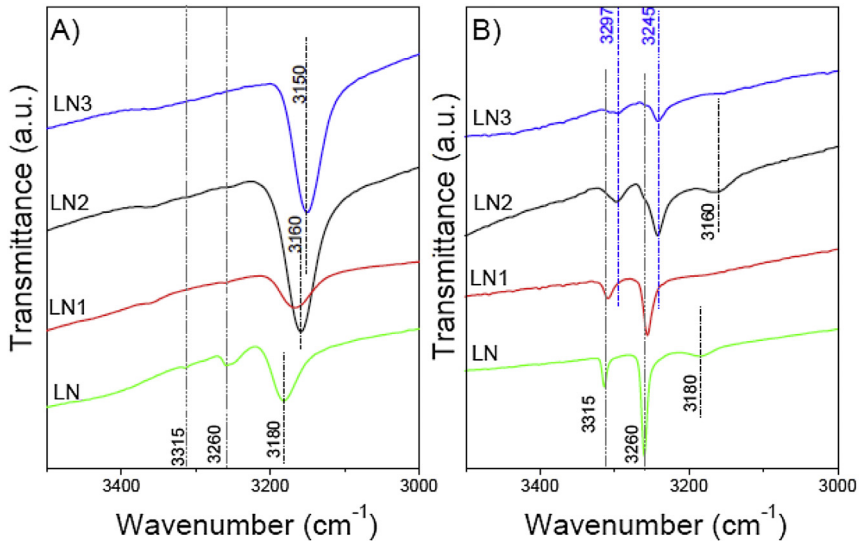

Fig. 5 – FTIR spectra of $AlCl_3$ doped $LiNH_2$-1.6LiH composite: (A) after dehydrogenation at 300 °C and 0.02 MPa and (B) after rehydrogenation at 300 °C and 0.7 MPa of hydrogen.

and 3245 cm^{-1} are clearly identified (Fig. 5B) and these are coincident with those observed after thermal treatment (Fig. 4B). Conversely, the band at 3365 cm^{-1} has completely disappeared.

These FTIR spectra constitute a confirmation of the hydrogen storage reversibility of the Li–Al–N–H–Cl system, with the amide-halide structure. However, it is important to remark that the first dehydrogenation process was accomplished for all doped samples (Fig. 2A), as it was indicated by the absence of the bands at 3260 and 3245 cm^{-1} (Fig. 5A). In addition, rehydrogenation was uncompleted for LN2 and LN3, as it can be inferred by the presence of the band at 3150 cm^{-1} (Fig. 4B). Then, both lithium aluminum amide-chloride and aluminum imide-chloride bands appear shifted with respect to the Li–N–H, in a way similar to previous observations [22].

From DSC, XRD and FTIR analysis, important differences were observed in the LN3 sample with respect to the other doped-systems. For this reason, LN3 was further submitted to thermal treatments coupled with XRPD and FTIR measurements. Fig. 6 shows XRPD patterns and FTIR spectra respectively, after heating at selected temperatures under argon and hydrogen. For comparison, the curve obtained for LN3 after milling is also shown (Fig. 6, curve I). As it was previously mentioned (Fig. 3B), in the as-milled LN3 XRPD pattern, the low angle peaks belonging to $LiNH_2$ seem to disappear and the most intense peaks are shifted towards lower angles. The FTIR curve of as-milled LN3 shows modifications of the N–H environment, as it can be inferred by the displacement of the bands at 3297 and 3245 cm^{-1} with respect to 3315 and 3260 cm^{-1} for pristine $LiNH_2$. However, structural information obtained from as-milled sample seems limited due to possible amorphization of LN3 during ball milling. When LN3 composite was heated 0.5 h under argon at 150 °C (Fig. 6A, pattern II), new diffraction peaks emerged at $2\theta = 12.0$, 14.47, 18.23, 20.9 and 22.6°. These peaks could be associated with those of the cubic and hexagonal $Li_4(NH_2)_3Cl$ phases. Moreover, the bands at 3297 and 3245 cm^{-1} are clearly identified and related with the $Li_4(NH_2)_3Cl$ type-phases (Fig. 6B, curve II). For LN3 specimen after 0.5 h of heat treatment under hydrogen at 300 °C (curve III), sharp XRPD peaks and FTIR bands in the same positions were obtained due to an increase of the crystallinity degree of the material.

These findings suggest that new species were generated after heating the sample to 150 °C, which can be assigned to a cubic phase isomorphous with $Li_4(NH_2)_3Cl$ ($a = 10.456$ Å). The presence of $Li_4(NH_2)_3Cl$-like phases indicates that a chemical reaction occurs in the as-milled material during heating under argon at 150 °C. Furthermore, as it is evidenced by the XRPD pattern in Fig. 3B, LiH is still present in the LN3 sample after the thermal treatment. This important detail can be associated with the fact that formation of the new amide-chloride-type phase is essentially ascribable to the reaction between $LiNH_2$ and $AlCl_3$. Considering that the formation of $Li_4(NH_2)_3Cl$ like phases occurred in the temperature range of the exothermic peak observed in the DSC (Fig. 1C) from as-milled LN3, this exothermic peak arises from the chemical reaction between $LiNH_2$ and $AlCl_3$. Further heating of LN3 for 12 h at 300 °C under hydrogen induces the trigonal/hexagonal phase to prevail (see Fig. 6B, curve IV). As a detail, an almost complete disappearance of the band at 3365 cm^{-1} is observed for all LN3 samples after heating. Remarkably, a novel synthesis route for type-$Li_4(NH_2)3Cl$ phases containing Al have been encountered.

Solid-state magic-angle spinning NMR was employed to investigate the chemical environments of Li and Al, both light elements, and to provide information on the processes involving hydride formation and their transformations. In particular, this technique will be powerful to demonstrate the incorporation of Al into amide/imide structure as well as the absence of free aluminum. Fig. 7A shows ^{7}Li MAS NMR spectra of the un-doped and $AlCl_3$ doped $LiNH_2$-1.6LiH composites after ball milling. The LN sample (dot dark curve)

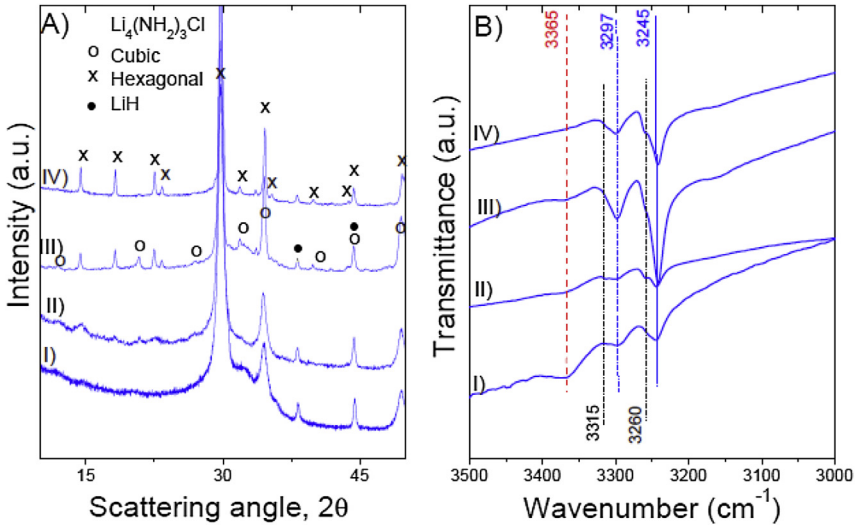

Fig. 6 – XRPD patterns (A) and FTIR spectra (B) of LN3 composite after: (I) 5 h of milling; (II) 0.5 h of heating at 150 °C under argon; (III) 0.5 h of heating at 300 °C under 0.7 MPa of hydrogen. (IV) 12 h of heating at 300 °C under 0.7 MPa of hydrogen.

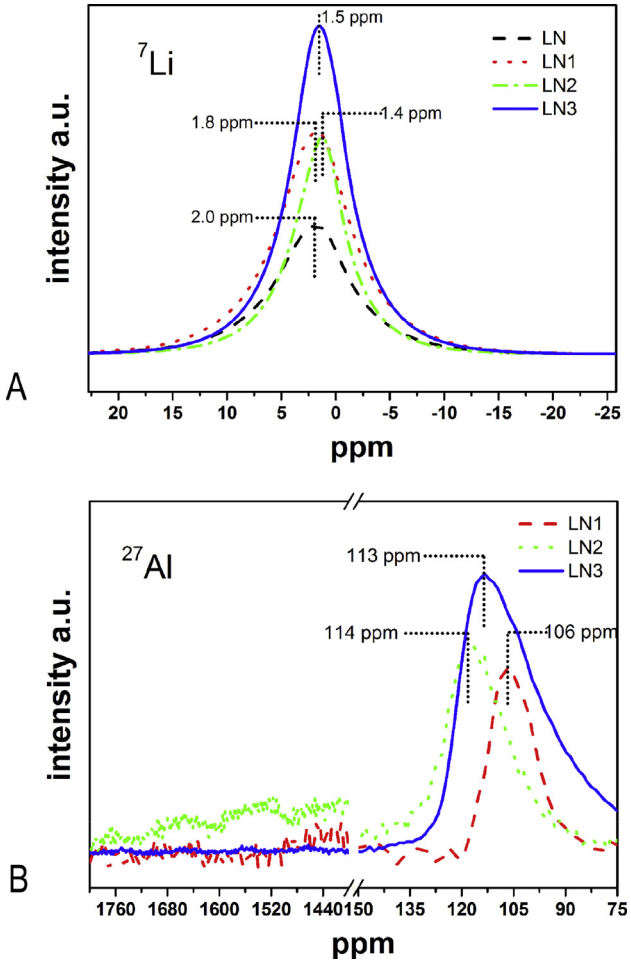

Fig. 7 – A) ^{7}Li MAS NMR spectra and B) ^{27}Al MAS NMR spectra of the LN, LN1, LN2 and LN3 composites after ball milling.

presents one dominant ^{7}Li NMR signal centered around 2.0 ppm, that can be easily resolved into two peaks placed at 3.0 and 1.1 ppm and associated to $LiNH_2$ [30] and LiH [31] phases, respectively, in agreement with XRPD studies (Fig. 3A). For the as-milled LN1 sample (red curvein web version) , the main peak is located at 1.8 ppm, and with respect to the un-doped sample, its position appears displaced to lower values of chemical shift. A further shift is observed for LN2 and LN3 composites, which display the main signals at 1.4 and 1.5 ppm, respectively. For the latter, a shoulder is also perceptible close to 0 ppm. The addition of $AlCl_3$ influenced the chemical environment of the Li specie, and the shift to lower field could be associated with the formation of a new local environment. Concerning the ^{27}Al NMR spectra (Fig. 7B), asymmetric peaks centered around 106, 114 and 113 ppm are detected for the samples LN1, LN2 and LN3, respectively. Interesting, no Al metallic signal (~1640 ppm [32,33]) is observed in the analysis, confirming its incorporation in the $LiNH_2$ lattice already after the mechanical treatment. These main signals typically appear at chemical shift values associated with Al–N–H species [29].

In Fig. 8, the ^{7}Li and ^{27}Al experiments on the thermally treated LN2 and LN3 are reported. Both LN2 and LN3 present one dominant ^{7}Li NMR peak at 1.22 and 1.34 ppm (Fig. 8A), respectively, further moved to lower chemical shift with respect to the as-milled samples. Regarding the ^{27}Al NMR spectra (Fig. 8B), a main peak centered at 116 ppm is detected for the LN2 sample, similar with that observed in Fig. 7B. Conversely, the ^{27}Al NMR profile of the LN3 sample in Fig. 8B, shows two main signals peaked at 120 and 113 ppm, respectively. Hence, it is possible to associate the NMR peak placed at 113 ppm to the hexagonal amide-chloride phase, taking into account that this is the only Al-based phase identified in the XRPD pattern in Fig. 3. Therefore, the second peak at 120 ppm is assigned to the cubic phase in accord with the corresponding XRPD analysis. Finally, similar to the

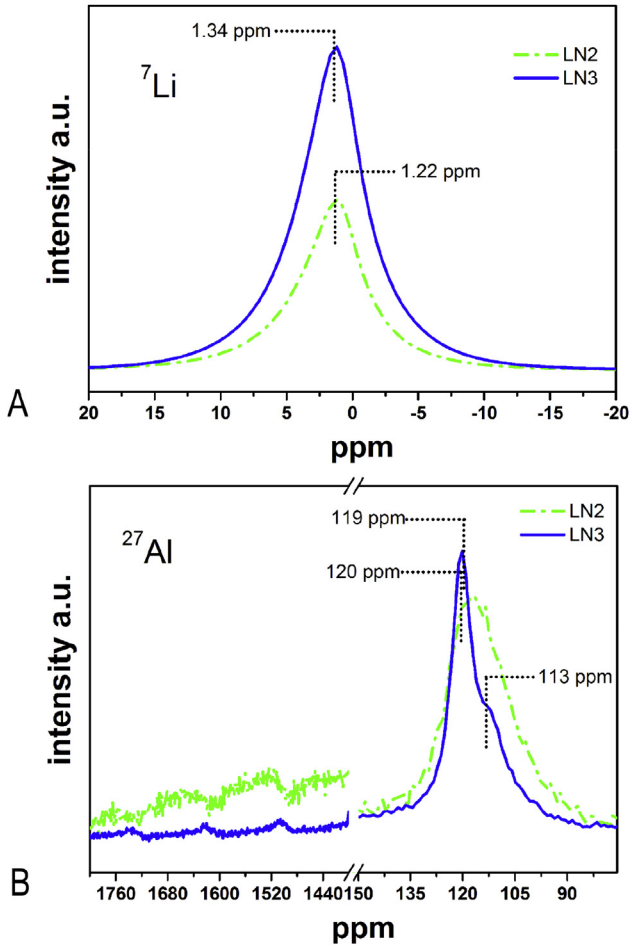

Fig. 8 – A) ^{7}Li MAS NMR spectra and B) ^{27}Al MAS NMR spectra of the LN2 and LN3 composites after annealing at 300 °C under 0.7 MPa of H_2.

milled samples, no Al metallic is detected upon the annealing treatment in the LN2 and LN3 composites.

The ^{7}Li NMR experiments on the desorbed composites are reported in Fig. 9A. The NMR spectrum of the LN1 composite after desorption is quite different with respect to that recorded for the as-milled sample (Fig. 7A). The chemical shift of the peak position is shifted from 1.8 (as milled LN1) to 3.9 ppm (first desorption of LN1). According to the literature [30,33], this chemical shift can be associated to the Li nucleus in the Li_2NH phase. The peak is characterized by a Lorentzian contribution and its profile, as well as the central peak/side bands intensity ratio, is quite similar to the ^{7}Li NMR of Li_2NH. The main peaks related to the LN2 and LN3 are shifted to lower chemical shift (2.3 and 3.1 pm) and their shapes resulted completely different with respect to the previous signal. This confirms that the environment of Li changes with respect to Li_2NH, in agreement with the previous XRPD and FTIR studies. Regarding the first re-hydrogenation cycle for LN1 composite (Fig. 9B), the peak centered position does not change significantly (1.6 versus 1.8 pm) compared to that observed for the as milled LN1 material, as well as the FWHM value (from 1081 to 1020 ppm). For rehydrogenated LN2 and LN3 composites (Fig. 9B), one main signal is detected, placed at 1.7 and 2.3 ppm, respectively. These chemical shifts turn out to be significantly displaced at lower field with respect to both the as-milled sample and that after the thermal treatment.

The ^{27}Al MAS NMR spectrum (Fig. 9C) of the dehydrogenated LN2 sample has a broad asymmetric peak located at 120 ppm, whereas the LN3 specimen shows two peaks at 113 and 119 ppm. Al-based new imide phases are expected to be formed during this step. Unfortunately, it is not possible to distinguish between amide and imide signals in this experiment, due to the broadening and the similar chemical shift of the two species. Finally, ^{27}Al MAS NMR spectra of the samples upon re-hydrogenation are reported in Fig. 9D. LN2 shows one main peak at 118 ppm, like to that observed in the as-milled and annealed samples. Similarly to the spectra recorded for the thermally treated LN3, the NMR pattern of the re-hydrogenated sample reports two peaks at 112 and 120 ppm, but with the signal intensity inverted. Hence, significant increase of the cubic phase can be surmised with respect to hexagonal one upon re-hydrogenation of the sample. The intensity inversion could be also explained by the un-reacted imide still present in the mixture. However, this is partially in contrast with the absorption test reported in Fig. 2B for the LN3 sample (97% of H_2 re-absorbed). Therefore, the first hypothesis appears to be the most acceptable.

Dehydrogenation thermodynamics and kinetics

According to the above results, it is possible to conclude that the interaction between $LiNH_2$–LiH and $AlCl_3$ induces relevant structural modifications in the Li–N–H system. For low $AlCl_3$ addition (0.03 mol), during milling Al^{3+} and Cl^- are incorporated into the $LiNH_2$ structure (represented by $LiAl_x(NH_2)Cl_{3x}$) resulting in an expansion of the lattice cell and in a modification of the chemical environment of Li, as it was demonstrated by XRPD and NMR, respectively. These structural changes remain in the material after further dehydrogenation/rehydrogenation, demonstrating the reversible Al^{3+} incorporation into $LiNH_2$. Considering that LiCl phase and/or the aluminum free are absent as inferred from XRPD and NMR measurements, respectively, the representative reactions can be expressed as follows:

After milling and further heating under hydrogen pressure:

$$LiNH_2(s) + x\ AlCl_3\ (s) + LiH(s) \rightarrow LiAl_x(NH_2)Cl_{3x}(s) + LiH(s) \quad (3)$$

During desorption/absorption:

$$LiAl_x(NH_2)Cl_{3x}(s) + LiH(s) \leftrightarrow Li_2Al_x(NH)Cl_{3x}(s) + H_2(g) \quad (4)$$

When extra amount of $AlCl_3$ is added to $LiNH_2$ (0.08 and 0.13 mol), milling and further thermal treatment under hydrogen lead to the formation of new amide-chloride phases, tentatively ascribed as Li–Al–N–H–Cl phases (represented by $Li_3Al_x(NH_2)_3Cl_{3x}$). XRPD studies demonstrate that these phases are isostructural with trigonal/hexagonal and cubic $Li_4(NH_2)_3Cl$, recently reported by Anderson [22]. Supposing

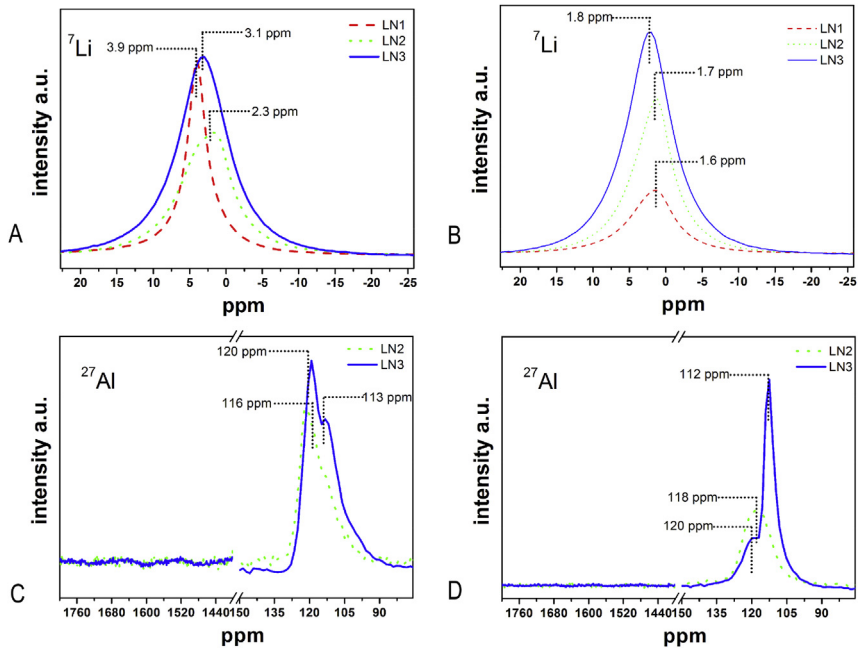

Fig. 9 – ^{7}Li MAS NMR spectra of the LN1, LN2 and LN3 composites after desorption (A) and re-absorption (B) measurements. ^{27}Al MAS NMR spectra of the LN1, LN2 and LN3 composites after desorption (C) and re-absorption (D) measurements.

that complete $AlCl_3$ incorporation occurs after milling and further thermal treatment, the reaction can be expressed:

$$LiNH_2(s) + x/3\ AlCl_3\ (s) + LiH(s) \rightarrow 1/3\ Li_3Al_x(NH_2)_3Cl_{3x} + LiH(s) \quad (5)$$

In particular, for the sample with 0.13 mol of $AlCl_3$, the formation of Li–Al–N–H–Cl phase after milling and further heating induces a chemical rearrangement at about 130 °C. Moreover, for the first time, FTIR and NMR measurements provide evidence about the presence of amide-chloride local environments containing Al. In fact, from FTIR the N–H stretches in $LiNH_2$ at 3315 and 3260 cm^{-1} are shifted to lower wave numbers at 3297 and 3245 cm^{-1} in Li–Al–N–H–Cl phases. Similarly, NMR measurements show that the Li chemical environment shifts to lower field, whereas new Al chemical shifts associated with Li–Al–N–H–Cl species appear at 120 and 113 ppm. No Al metallic is detected upon the annealing, dehydrogenation or hydrogenation of the LN2 and LN3 composites.

Considering that $AlCl_3$ doped samples display improved hydrogen storage properties (Figs. 1 and 2) in connection with the relevant structural changes observed (Figs. 3–9), it is of relevance to analyze the relative thermodynamic stability and the dehydrogenation kinetics of these composites. Regarding thermodynamics behavior, dehydrogenation PCI curves of the LN and doped-LN samples at 300 °C are shown in Fig. 10. For LN, the isotherm displays an initial plateau up to ~2.3 wt.% of hydrogen, in the pressure range between 0.28 and 0.19 MPa. After this, the data begins to slope down toward the complete dehydrogenation. This sloping behavior in the PCI curve of the $LiNH_2$–LiH system can be interpreted by recent investigations [23,26]. David et al. [23] accounted that while $LiNH_2$ is the dominant phase in the hydrogenated state, phases with intermediate stoichiometry between $LiNH_2$ and Li_2NH might exist in the dehydrogenated state. On this base, a Frenkel defect model based on the migration of Li^+ and H^+ ions for dehydrogenation (and hydrogenation) and the formation of NH_3 was proposed. This mechanism has been recently confirmed by Makepeace et al. [34] by *in situ* synchrotron X-ray powder diffraction experiments, where the formation and evolution of non-stoichiometric intermediate species of the form $Li_{1+x}NH_{2-x}$ was demonstrated. In this last work, it was also proved the reduced stability of intermediate stoichiometry values ($0.4 \leq x \leq 0.7$) compared with the end member species $LiNH_2$ and Li_2NH. Then, the sloping behavior of the PCI curve can be related with the conversion of $LiNH_2$ into Li_2NH, involving the formation of non-stoichiometric species.

In the case of $AlCl_3$-doped composites, the dehydrogenation of LN1 can be represented by reaction (4), which looks similar than reaction (1). By comparison of PCI curve of LN1 with LN, it can be seen that for LN1, the hydrogen pressure

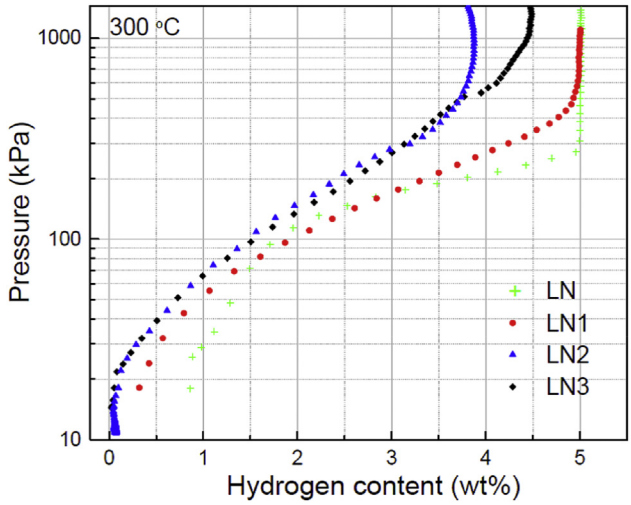

Fig. 10 – PCIs of $AlCl_3$ doped $LiNH_2$-1.6LiH systems dehydrogenated at 300 °C. LN analysis is reported for comparison.

decreases monotonically with the amount of hydrogen released from 0.48 MPa, with the consequent absence of a well-defined plateau. This suggests the existence of non-stoichiometry phases in the complete range from $LiAl_x(NH_2)Cl_{3x}$ to $Li_2Al_x(NH)Cl_{3x}$, according reaction (4). In the case of LN2 and LN3, the PCIs measured represent the thermodynamic behavior of the amide-chloride phases containing Al, which is reported for the first time. In both cases, the hydrogen pressure decreases with the amount of hydrogen released, suggesting the existence of non-stoichiometric phases of unknown nature. The onset hydrogen equilibrium pressure for the amide-halide phases was about 0.62 MPa.

To determine the activation energy for the dehydrogenation process of the doped and un-doped composites, Kissinger method was employed (Figs. S2 and S3). The apparent activation energy was found to be 109 ± 3 (LN1), 122 ± 4 (LN2) and 125 ± 3 (LN3) kJ/mol for the doped composites and 113 ± 5 kJ/mol for the un-doped material, respectively. Although the values for LN and LN1 are within the error bar of the method applied (113 vs. 109 kJ/mol), the activation energies for the LN2 and LN3 samples (122 and 125 kJ/mol) turns out to be higher beyond uncertainty. Typically, a change in the activation energy can be related to a change in the reaction mechanism or in the energy state of the reactants. Considering the higher values of E_a obtained for LN2 and LN3 respect LN, and their enhanced dehydrogenation rates (Fig. 2), both possibilities could be viable for the amide-chloride phases.

Finally, it is noteworthy that all doped-$AlCl_3$ samples display enhanced hydrogen storage properties in comparison with $LiNH_2$–LiH. Although the higher onset equilibrium pressures at 300 °C for doped system suggest the thermodynamic destabilization of $LiNH_2$–LiH, the improvements dehydrogenation kinetics are more noticeable. Also, the $AlCl_3$-doped samples resulted in significant suppression of ammonia release. For low $AlCl_3$ amount, Al^{3+} incorporation into $LiNH_2$ structure produces an expansion in the lattice, favoring the mobility of Li^+ and H^+ ions and consequently enhancing the dehydrogenation rate via the topotactic mechanism [22]. However, no clear modification in the activation energy was observed. The situation for high amount of $AlCl_3$ added to $LiNH_2$ looks different. New phases type amide-chloride and imide-chloride were formed in the hydrogenated and dehydrogenated states, respectively. From the PCIs and kinetics studies it is expected a different thermodynamic stability and dehydrogenation controlling mechanism for these new phases, which need to be determined. However, the improved hydrogen sorption properties observed can be ascribed to an enlargement of Li^+ mobility in the new chloride-amide phases and the weakening of the N–H bond due to the incorporation of Al^{3+} and Cl^- in the lattice.

Conclusions

In this work, the hydrogen storage properties of the $AlCl_3$ doped $LiNH_2$-1.6LiH composites were investigated. All $AlCl_3$-doped samples exhibited advantageous hydrogen storage performance. The dehydrogenation rate from these composites was three-fold and six-fold faster than for un-doped $LiNH_2$-1.6LiH, depending of the Al content in the sample. The rehydrogenation kinetics is also faster for doped material, conducting to good reversibility. In addition, a notable reduction/elimination of the NH_3 emission was also shown.

Structural analyses performed by XRPD, FTIR and NMR demonstrated the interactions that occur between $AlCl_3$ and $LiNH_2$-1.6LiH during milling, dehydrogenation and hydrogenation. For low amount addition of $AlCl_3$, Al^{3+} is incorporated into $LiNH_2$ lattice whereas for high amount of $AlCl_3$, new amide-chloride phases belonging to the Li–Al–N–H–Cl system are formed. The new phases were assigned to both hexagonal and cubic phases, isomorphous with $Li_4(NH_2)_3Cl$ compounds. The mechanism that enhances the hydrogen sorption properties depends upon the structural modifications introduced in the Li–N–H system. The inclusion of Al^{3+} in the $LiNH_2$ favors the mobility of the Li^+ and H^+ ions into $LiNH_2$ lattice. Moreover, the addition of high amount of $AlCl_3$ leads to the formation of new amide-chloride aluminum phases. These new phases promote not only Li^+ migration during dehydrogenation kinetics, but also a red shift of the N–H bond with respect to $LiNH_2$, indicating a weakening of N–H bonding. Their thermodynamic stability is unknown up today.

Acknowledgment

S.G. gratefully acknowledges the COST Action MP1103: "Nanostructured Materials for Solid State Hydrogen Storage", for the financial support. M.D.B. acknowledges financial support from an ICREA-Academia Award and the 2014 SGR 1015 project from the Generalita de Catalunya. This study has been partially supported by bilateral collaboration Project MINCyT-MAE. L.F.A., P.A.L. and F.G. acknowledge CONICET (National Council of Scientific and Technological Research), CNEA (National Commission of Atomic Energy), ANPCyT (Project N° 1052) and Instituto Balseiro (University of Cuyo).

Appendix A. Supplementary data

Supplementary data related to this article can be found at http://dx.doi.org/10.1016/j.ijhydene.2015.08.030.

REFERENCES

[1] Bogdanović B, Schwickardi M. Ti-doped alkali metal aluminum hydrides as potential novel reversible hydrogen storage materials. J Alloys Compd 1997;253–254:1–9.

[2] Bogdanović B, Felderhoff M, Kaskel S, Pommerin A, Schlichte K, Schüth F. Improved hydrogen storage properties of Ti-doped sodium alanate using titanium nanoparticles as doping agents. Adv Mater 2003;15:101210–5.

[3] Urbanczyk R, Peinecke K, Felderhoff M, Hauschild K, Kersten W, Peil S, et al. Aluminium alloy based hydrogen storage tank operated with sodium aluminium hexahydride Na_3AlH_6. Int J Hydrogen Energy 2014;39:17118–28.

[4] Böesenberg U, Doppiu S, Mosegaard L, Borgschulte A, Eigen N, Barkhordarian G, et al. Hydrogen sorption properties of MgH_2+2$LiBH_4$. Acta Mater 2007;55:3951–8.

[5] Pistidda C, Garroni S, Minella CB, Dolci F, Jensen TR, Nolis P, et al. Pressure effect on the 2NaH + MgB2 hydrogen absorption reaction. J Phys Chem C 2010;114:21816–23.

[6] Jepsen J, Milanese C, Girella A, Lozano G, Pistidda C, Bellosta von Colbe J, et al. Compaction pressure influence on material properties and sorption behaviour of $LiBH_4$–MgH_2 composite. Int J Hydrogen Energy 2013;38:8357–66.

[7] Gennari FC. Improved hydrogen storage reversibility of $LiBH_4$ destabilized by $Y(BH_4)_3$ and YH_3. Int J Hydrogen Energy 2012;37:18895–903.

[8] Chen P, Xiong Z, Luo J, Lin J, Tan LT. Interaction of hydrogen with metal nitrides and imides. Nature 2002;420:302–4.

[9] Zhang Y, Xiong Z, Cao H, Wu G, Chen P. The enhanced hydrogen storage performance of (Mg–B–N–H)-doped $Mg(NH_2)$–2LiH system. Int J Hydrogen Energy 2014;39:1710–8.

[10] Kojima Y, Matsumoto M, Kawain Y, Haga T, Ohba N, Miwa K, et al. Hydrogen absorption and desorption by the Li-Al-N-H system. J Phys Chem B 2006;110:9632–6.

[11] Markmaitree T, Ren R, Shaw L. Enhancement of lithium amide to lithium imide transition via mechanical activation. J Phys Chem B 2006;110:20710–8.

[12] Yao JH, Shang C, Aguey-Zinsou KF, Guo ZX. Desorption characteristics of mechanically and chemically modified $LiNH_2$ and ($LiNH_2$+LiH). J Alloys Compd 2007;432:277–82.

[13] Yang J, Li D, Fu H, Xin G, Zheng J, Li X. In situ hybridization of $LiNH_2$–LiH–$Mg(BH_4)_2$ nano-composites: intermediate and optimized hydrogenation properties. Phys Chem Chem Phys 2012;14:2857–63.

[14] Nayebossadri S, Aguey-Zinsou KF, Yao J, Guo ZX. Effect of nitride additives on Li-N-H storage system. Int J Hydrogen Energy 2011;36:7920–6.

[15] Isobe S, Ichikawa T, Hanada N, Leng HY, Fichtner M, Fuhr O, et al. Effect of Ti catalyst with different chemical form on Li-N-H hydrogen storage properties. J Alloys Compd 2005;404:439–42.

[16] Sale M, Pistidda C, Taras A, Napolitano E, Milanese C, Karimi F, et al. In situ synchrotron radiation powder X-ray diffraction study of the 2$LiNH_2$ + LiH + KBH_4 system. J Alloys Compd 2013;580:S278–81.

[17] Valentoni A, Garroni S, Pistidda C, Masolo E, Napolitano E, Moretto P, et al. New insights into the thermal desorption of the 2$LiNH_2$ + KBH_4 + LiH mixture. Int J Hydrogen Energy 2014;39:17075–82.

[18] Ulmer U, Hu J, Fransreb M, Fichtner M. Preparation, scale-up and testing nanoscale, doped amide systems for hydrogen storage. Int J Hydrogen Energy 2013;38:1439–49.

[19] Amica G, Arneodo Lorochette P, Gennari FC. Hydrogen storage properties of $LiNH_2$–LiH system with MgH_2, CaH_2 and TiH_2 added. Int J Hydrogen Energy 2015;40:9335–46.

[20] Zhang J, Hu YH. Decomposition of lithium amide and lithium imide with and without anion promoter. Ind Eng Chem Res 2011;50:8058–64.

[21] Leng H, Wu Z, Duan W, Xia G, Li Z. Effect of $MgCl_2$ additives on the H-desorption properties of Li-N-H system. Int J Hydrogen Energy 2012;37:903–7.

[22] Anderson AA, Chater PA, Hewett DR, Slater PR. Hydrogen storage and ionic mobility in amide-halide systems. Faraday Discuss 2011;151:271–84.

[23] David WIF, Jones MO, Gregory DH, Jewell CM, Johnson SR, Walton A, et al. A mechanism for non-stoichiometry in the lithium amide/lithium imide hydrogen storage reaction. J Am Chem Soc 2007;129:1594–601.

[24] Fernández Albanesi L, Arneodo Lorochette P, Gennari FC. Destabilization of the $LiNH_2$–LiH hydrogen storage system by aluminum incorporation. Int J Hydrogen Energy 2013;38:12325–34.

[25] Maud - Materials Analysis Using Diffraction, http://www.ing.unitn.it/~maud/index.html [accessed November 2014].

[26] Lutterotti L. Total pattern fitting for the combined size-strain-stress-texture determination in thin film diffraction. Nucl Instrum Methods Phys Res B 2010;268:334–40.

[27] Hewett DR. Mixed anion amides for hydrogen storage [Ph.D. thesis]. University of Birmingham; 2012. Research archive e-theses repository.

[28] Xiong Z, Wu G, Hu J, Liu Y, Chen P, Luo W, et al. Reversible hydrogen storage by a Li-Al-N-H complex. Adv Funct Mater 2007;17:1137–42.

[29] Janot R, Eymery JB, Tarascon JM. Decomposition of $LiAl(NH_2)_4$ and reaction with LiH for a possible reversible hydrogen storage. J Phys Chem C 2007;111:2335–40.

[30] Jun L, Fang ZZ, Sohn HY, Bowman Jr RC, Hwang SJ. Potential and reaction mechanism of Li-Mg-Al-N-H system for reversible hydrogen storage. J Phys Chem C 2007;111:16686–92.

[31] Choi YJ, Jun Lu J, Sohn HJ, Fang ZZ, Kim C, Bowman Jr RC, et al. Reaction mechanisms in the Li_3AlH_6/$LiBH_4$ and Al/$LiBH_4$ systems for reversible hydrogen storage. Part 2: solid-state NMR studies. J Phys Chem C 2011;115:6048–56.

[32] Soru S, Taras A, Pistidda C, Milanese C, Bonatto Minella C, Masolo E, et al. Structural evolution upon decomposition of the $LiAlH_4$ + $LiBH_4$ system. J Alloys Compd 2014;615:S693–7.

[33] Dolotko O, Zhang H, Ugurlu O, Wiench JW, Pruski M, Scott Chumbley L, et al. Mechanochemical transformations in Li(Na)AlH_4-Li(Na)NH_2 systems. Acta Mater 2007;55:3121–30.

[34] Makepeace JW, Jones MO, Callear SK, Edwards PP, David WDIF. In situ X-ray powder diffraction studies of hydrogen storage and release in the Li–N–H system. Phys Chem Chem Phys 2014;16:4061–70.